

# AERODYNAMIC MODEL IDENTIFICATION OF A VTOL TAILSITTER UAV USING SPARSE IDENTIFICATION OF NONLINEAR DYNAMICS

Hosun Lee<sup>1</sup>, Jayden Dongwoo Lee<sup>1</sup> & Hyochoong Bang<sup>1</sup>

<sup>1</sup>Department of Aerospace Engineering, KAIST, Daejeon, Republic of Korea

# **Abstract**

A tailsitter unmanned aerial vehicle (UAV) enables efficient cruise flight along with vertical take-off and landing (VTOL) capabilities without extra mechanisms for a transition maneuver. Flight envelope of the tailsitter includes a post-stall range, which makes its aerodynamic model highly nonlinear and difficult to identify. Moreover, control inputs from elevons and propellers are inherently coupled with the aerodynamic model. Thus, it is essential to obtain an accurate aerodynamic model to achieve precise control of the system. As a data-driven approach, a sparse identification of nonlinear dynamics (SINDy) is applied to identify the aerodynamic model of the tailsitter UAV. SINDy can learn nonlinear dynamics from noisy measurement data and balance accuracy with model complexity to avoid overfitting by sparsifying the space of composing equations. By utilizing the minimum knowledge of the model, the aerodynamic model is constructed from measurement data and the overall system is fully derived. As a result, the aerodynamic forces and moments are expressed as nonlinear functions of system states. We present results of numerical simulation and application of the derived model into feedback linearization controller.

Keywords: SINDy, System Identification, Tailsitter UAV, Aerodynamic Model

## 1. Introduction

A tailsitter is one of unmanned aerial vehicles (UAV) configurations with vertical take-off and landing (VTOL) capability. The tailsitter takes off and lands vertically on its tail and tilts the entire airframe horizontally to achieve cruise flight [1]. Due to its VTOL characteristics, it has three distinct flight phases which are hover, transition, and cruise flight as shown in Fig. 1. In hover phase, the vehicle hovers vertically by the thrust generated by propellers which is same with rotary-wing aircrafts. The transition flight is an intermediate phase between hover and cruise phase [2]. Pitch is tilted along with a wide variation in horizontal velocity. Forward transition refers to a transition from hover to cruise flight and the vehicle performs pitch down for about 90°. Backward transition refers to the vice versa. The vehicle pitches up for about 90° and changes from cruise to hover flight. During the cruise phase, it flies in near-horizontal attitude with efficient lift production from the main wing like the conventional fixed-wing UAVs.

The tailsitter has distinct advantages over multicopters and fixed-wing aircrafts due to its unique flight mechanism. Compared to multicopters, the tailsitter has longer endurance time and operational range because its lift is generated from the main wing during cruise flight. Due to its efficient forward flight, the operational range and versatility can be extended. Compared to fixed-wing aircrafts, the operational environment can be broadened to a narrow and confined area, allowing full operational autonomy [3]. One distinct feature of the tailsitter from other VTOLs is the absence of extra mechanism for changing the direction of propulsion system. Unlike tilt-rotors or tilt-wing VTOLs that have mechanical devices for tilting rotors or wings, the tailsitter is operable without any additional tilting devices. It typically utilizes a set of propellers and control surfaces that can cover the entire flight phases. It gives mechanical simplicity along with light-weight and decreased susceptibility to hardware failures [4].

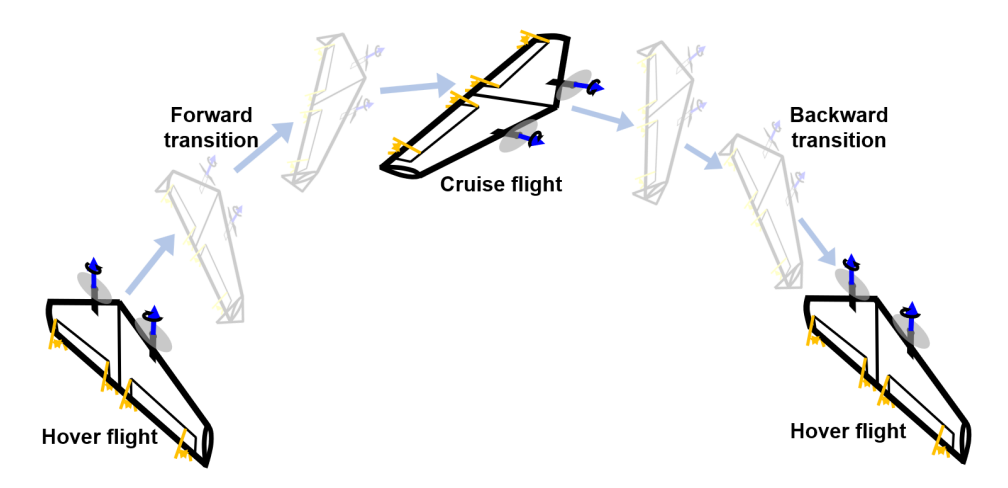


Figure 1 – Flight modes of a tailsitter UAV.

However, the advantage in simple mechanism acts as difficulties in the perspective of control. Due to its structural configuration, the control forces and moments are coupled with aerodynamic effects of the main wing. Specifically, the pitching moment during the transition flight is affected by aerodynamic moments. In addition, the flight envelope includes a post-stall area with a wide range of angle of attack [1]. It induces nonlinear and complex aerodynamic model with unknown lift and drag coefficients. The unknown aerodynamic forces and moments act as uncertainties in the system model, which degrades the control performance. For a tailsitter with dual-rotor configuration, control inputs can be expressed as a nonlinear function of vehicle velocity, control surface deflection angle, and thrust. In order to control such system, the nonlinear relations should be revealed through accurate modeling. Therefore, the importance of identifying precise aerodynamic model is magnified.

System identification is the process of building mathematical models for dynamic systems using imperfect measurements of the systems. Several approaches have been introduced for the system identification of aerodynamic model of UAVs. In [5] and [6], dependent Gaussian process is introduced to estimate the aerodynamic coefficients of fixed-wing aircrafts. The proposed algorithms learned the force and moment coefficients from real flight data. However, they do not consider the aerodynamic model in post-stall region. Extended Kalman filter is used to estimate the aerodynamic parameters of a flying wing tailsitter in [4] and a sequentially thresholded least squares algorithm is suggested to find an aerodynamic model of a fixed-wing UAV in [7]. In [8], Extended and unscented Kalman filter is used to estimate aerodynamic parameter of fixed-wing aircrafts from real flight data. In [9], Dynamic mode decomposition with control is applied to attain aerodynamic parameters of a sub-scale jet transport aircraft. However, limitations still exist in the aerodynamic model of the tailsitter because it is more complex on post-stall region and learning multiple outputs while capturing dependencies is required.

There have been work done on identifying the aerodynamic model of tailsitter vehicles. In [10], non-linearities of a tailsitter during transition are estimated with Neural Network. The aerodynamic forces are well estimated, which improved control performance, but a significant amount of data was needed for network construction. Additionally, several tailsitter researches conducted wind tunnel tests in [3] and [11]. However, the previous approaches have drawbacks to some extent. Wind tunnel testing is labor intensive and is only applicable to a narrow flight envelope. And model-based system identification approaches require prior knowledge of the model structure. And the Neural networks require a considerable amount of training data and time to learn the model. Also, it has longer execution time compared to SINDy [12]. For the tailsitter platform, these drawbacks are critical in that collecting abundant flight data is practically difficult due to the limitations on maneuvering. Moreover, the data should be obtained without knowing exact aerodynamic model, which makes stable flight difficult. The frequency of a feedback control loop should be kept fast enough to keep the vehicle stable and it does not give sufficient computing time for any algorithms.

To solve those challenges, a data-driven based approach is suggested in this paper. Sparse Identification of Nonlinear Dynamics (SINDy) algorithm provides a data-driven model discovery framework, resulting in interpretable models that avoid overfitting, relying on sparsity-promoting optimization to identify parsimonious models from limited data. In [13], [14], and [15], SINDy is introduced to discover an unknown model from the data. In [12], a sparse identification of nonlinear dynamics with control (SINDYc) considering both system states and control inputs is introduced with backstepping control method. The SINDYc is compared with Neural network and it showed higher prediction accuracy and stronger generalization ability. In [16] and [17], a data-driven SINDy method is extended to obtain the dynamic model of serial manipulators and 6DOF spatial manipulators. The identified model accurately replicated the performance of the robot in the simulation and experiments when different levels of noise are added to the data. In [18], SINDy is implemented in the quadrotor system, including the gyroscopic and aerodynamic effect. Also, SINDy is combined with sliding mode controller to get accurate and low complexity model of end-effector positioning of a soft robot in [19].

The precise dynamic model of the tailsitter is hard to attain, motivating the application of SINDy algorithm to learn an accurate and sparse model from flight test data. Therefore, in this paper, the identification of the aerodynamic model of a tailsitter will be conducted using SINDy.

This paper is structured as follows: In Section 2, the dynamic model of a tailsitter with flying wing configuration is described. The methodology of sparse identification of nonlinear dynamics and its formulation for aerodynamic model identification is presented in Section 3. Simulation results of the proposed methodology are given in Section 4 along with the results with controller using the constructed model. Finally, the summary and conclusion will be addressed in Section 5.

### 2. Problem Formulation

# 2.1 Coordinates

The body-fixed and inertial coordinate frames are defined in Fig. 2 For the inertial frame I, North-East-Down (NED) convention is used where  $x_I$  is North,  $y_I$  is east, and  $z_I$  is down. The body-fixed coordinates B follow conventional fixed-wing aircraft notation with the origin located at the center of gravity.  $x_B$  is forward direction in the fixed-wing configuration, which is perpendicular to the propeller plane,  $y_B$  is the right wing direction, and  $z_B$  is downward direction expressed as  $z_B = x_B \times y_B$ .

### 2.2 Flying Wing Tailsitter Model

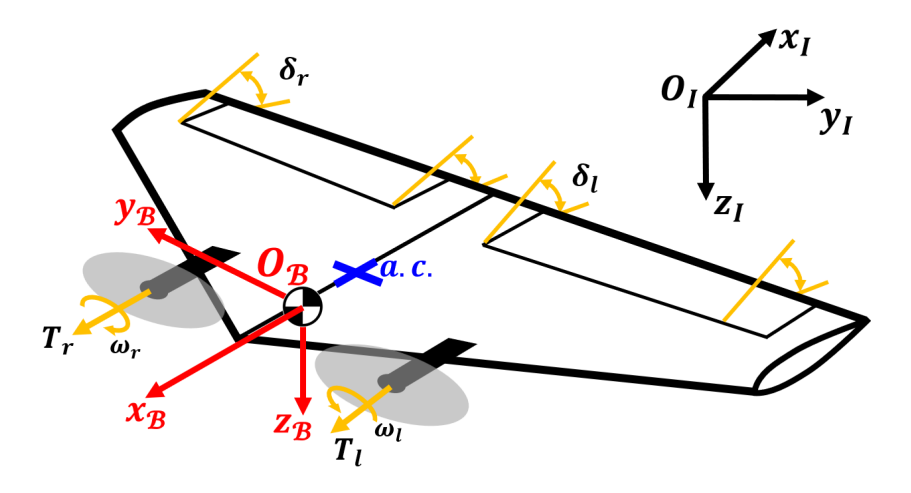


Figure 2 – Illustration and coordinates of a flying wing tailsitter UAV.

The tailsitter model has a dual-rotor flying wing configuration as shown in Fig. 2. It is designed to have two rotors and two elevons on the left and right wing each to maximize mechanical simplicity. Two rotors are mounted on the leading edge of the left and right wing, respectively. The motors turn each rotors in opposite direction to compensate angular momentum in  $z_B$  axis.  $T_l$  and  $T_r$  are the primary and unique thrust source of the vehicle and acts in  $x_B$  direction. Also, differential thrust of the rotors can generate moment in  $z_B$  axis. As control surfaces, elevons are located on the trailing edge of the

Table 1 – Tailsitter UAV properties

Property	Symbol	Value
Airfoil	-	NACA0012
Mass	m	709g
Aspect ratio	AR	2.96
Sweep angle	γ	25.21°
Mean chord length	$\bar{c}$	310 <i>mm</i>
Wing surface area	Swing	$0.26m^2$
Elevon surface area	Selv	$0.06m^2$
Distance to center of gravity	$x_{cg}$	57.5mm
Distance to aerodynamic center	x <sub>ac</sub>	77.5mm
Propeller radius	$R_{prop}$	63.5 <i>mm</i>
Propeller moment arm	$l_{prop}$	120 <i>mm</i>
Propeller reaction torque coefficient	$c_Q$	$2.4e$ - $6Nm/rad^2$

left and right wing. The elevons generate moment in  $x_B$  and  $y_B$  axis through deflection to opposite or same direction. The deflection angle of left and right elevons are denoted as  $\delta_l$  and  $\delta_r$  each and positive deflection corresponds to downward direction. Unlike conventional aircrafts, we assume the elevons are always effective with unstalled condition. It is achievable since the propeller-induced airflow can produce a steady flow without separation from the main wing. Therefore, the elevons can generate moment in hovering or post-stall condition [11]. And in order to generate sufficient moments for transition flight, the elevons are designed to have larger surface compared with conventional flying wing aircrafts. The detailed properties of the tailsitter UAV is summarized in Table. 1

During the cruise flight, the flying wing model is designed to have longitudinal and directional stability. As shown in Fig. 3, The upward trim of elevons  $\delta_{\text{trim}}$  makes the symmetric airfoil to have reflexed camber line. It makes the positive pitching moment  $M_{0.25}^*$  at the aerodynamic center. Overall,  $M_{0.25}^*$  makes the moment equilibrium combined with the weight at the center of gravity and the lift force at the aerodynamic center. Since the center of gravity is located in front of the aerodynamic center, it can ensure longitudinal stability in disturbed states also. And the differential induced drag from the sweep back angle can provide directional stability.

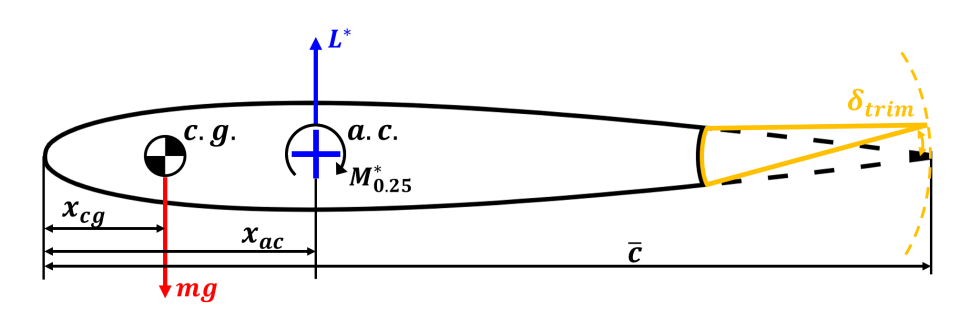


Figure 3 – Illustration of airfoil cross-section in equilibrium state.

### 2.3 Dynamics of the Tailsitter

Let us define  $\mathbf{v}_B = [u, v, w]^T$  and  $\mathbf{p}_I = [x_I, y_I, z_I]^T$  be the vehicle velocity in the body frame and position in the inertial frame.  $\omega_B = [p, q, r]^T$  is angular velocity in the body frame and  $\phi$ ,  $\theta$ ,  $\psi$  are the Euler angles to represent attitude.  $\alpha = \tan^{-1}(\frac{w}{u})$  is the angle of attack (AOA) and  $\beta = \sin^{-1}(v/\sqrt{u^2 + v^2 + w^2})$  is the angle of sideslip. Then, the system states and control inputs are defined as:

$$\mathbf{x} = [u, v, w, p, q, r, x_I, y_I, z_I, \phi, \theta, \psi, \alpha, \beta]^T,$$

$$\mathbf{u} = [T_I, T_r, \delta_I, \delta_r]^T,$$
(1)

where  $T_l, T_r$  correspond to the left and right rotor thrust each and  $\delta_l, \delta_r$  are the left and right elevon deflection angle, respectively.

The tailsitter vehicle is modeled as a rigid body with the mass m and the moment of inertia  $\mathbf{J} = diag\{J_{xx}, J_{yy}, J_{zz}\}$  where  $\mathbf{J}$  is a diagonal matrix. The dynamics of the tailsitter can be expressed in Newton-Euler equations as:

$$m\dot{\mathbf{v}}_{I} = {}^{B}\mathbf{R}_{I}^{T}\mathbf{F}_{B} + m\mathbf{g}_{I},$$
  

$$\mathbf{J}\dot{\omega}_{B} = \mathbf{M}_{B} - \omega_{B} \times \mathbf{J}\omega_{B},$$
(2)

where  $\mathbf{g}_I = [0, 0, g]^T$  is the gravitational acceleration and  ${}^B\mathbf{R}_I$  represent a rotation matrix from I to B.  $\mathbf{F}_B$  and  $\mathbf{M}_B$  denotes the force and moment acting on the vehicle, respectively.

The force **F** and moment **M** exerted in the body frame can be decomposed as wing, propeller, and elevon components as:

$$\begin{aligned} \mathbf{F} &= \mathbf{F}_{\text{wing}} + \mathbf{F}_{\text{prop}} + \mathbf{F}_{\text{elv}}, \\ \mathbf{M} &= \mathbf{M}_{\text{wing}} + \mathbf{M}_{\text{prop}} + \mathbf{M}_{\text{elv}}. \end{aligned} \tag{3}$$

where  $(*)_{wing}$  denotes the aerodynamic component from the main wing without elevon effects. It describes forces and moments when elevon deflection angle is fixed at  $\delta_{trim}$ .  $(*)_{prop}$  denotes the propeller component and  $(*)_{elv}$  represents the extra effect due to elevon deflection. All of three components can be seen as aerodynamic terms in that the forces and moments are produced by interaction with airflow.

# 2.3.1 Main Wing Model

The lift, drag, and pitching moment are produced from the main wing model. Since the vehicle has flying wing configuration without tail stabilizers, we can reasonably ignore the force in  $y_B$  and moments in  $x_B$  and  $z_B$ . The active terms in the body frame can be represented as;

$$\mathbf{F}_{\text{wing}} = \begin{bmatrix} F_{\text{wing,x}} \\ F_{\text{wing,z}} \end{bmatrix} = \begin{bmatrix} L\sin\alpha - D\cos\alpha \\ 0 \\ -L\cos\alpha - D\sin\alpha \end{bmatrix},$$

$$\mathbf{M}_{\text{wing}} = \begin{bmatrix} L_{\text{wing}} \\ M_{\text{wing}} \\ N_{\text{wing}} \end{bmatrix} = \begin{bmatrix} 0 \\ M_{\text{pitch}} - (L\cos\alpha + D\sin\alpha)(x_{\text{ac}} - x_{\text{cg}}) \\ 0 \end{bmatrix},$$

$$(4)$$

$$\begin{split} L &= \bar{q} \, s_{\mathsf{Wing}} C_L(\alpha), \\ D &= \bar{q} \, s_{\mathsf{Wing}} C_D(\alpha), \\ M_{\mathsf{pitch}} &= \bar{q} \, s_{\mathsf{Wing}} \bar{c} \, C_M(\alpha), \end{split} \tag{5}$$

where L and D are the lift and drag force each,  $M_{\text{pitch}}$  denotes the pitching moment of the main wing. The dynamic pressure is  $\bar{q} = \frac{1}{2}\rho V_T^2$  with air density  $\rho$  and total velocity of the vehicle  $V_T = \sqrt{u^2 + v^2 + w^2}$ .  $C_L(\alpha), C_D(\alpha), C_M(\alpha)$  are unknown nonlinear functions of aerodynamic coefficients.

# 2.3.2 Propeller Model

The propellers generate outflow of the air that makes force in  $x_B$  direction. Since two propellers are attached in  $x_B$  direction facing forward, they also induce moments in  $x_B$  and  $z_B$  direction through differential thrust. From the classical momentum theory [20], the inflow and outflow velocity of the propellers are

$$V_{\text{in}} = \frac{V_T \cos \alpha + V_{\text{out}}}{2},$$

$$V_{\text{out}} = \sqrt{\frac{T_l + T_r}{\rho \pi R_{\text{prop}}^2} + (V_T \cos \alpha)^2}.$$
(6)

The outflow with  $V_{\text{out}}$  makes artificial airflow toward the elevons, producing unseparated airflow which makes the elevons work as effective control inputs for the entire flight envelopes.

The force and moment of the propellers are

$$\mathbf{F}_{\mathsf{prop}} = \begin{bmatrix} F_{\mathsf{prop},\mathsf{x}} \\ F_{\mathsf{prop},\mathsf{y}} \\ F_{\mathsf{prop},\mathsf{z}} \end{bmatrix} = \begin{bmatrix} T_l + T_r \\ 0 \\ 0 \end{bmatrix},$$

$$\mathbf{M}_{\mathsf{prop}} = \begin{bmatrix} L_{\mathsf{prop}} \\ M_{\mathsf{prop}} \\ N_{\mathsf{prop}} \end{bmatrix} = \begin{bmatrix} c_{\mathcal{Q}}(-T_l + T_r) \\ 0 \\ l_{\mathsf{prop}}(T_l - T_r) \end{bmatrix}.$$

$$(7)$$

### 2.3.3 Elevon Model

In order to make the elevons effective on post-stall region, we design the elevons to be covered by outflow of propellers. With this assumption, we can construct the elevon model similar to conventional fixed-wing model. The force and moment of the elevons are

$$\mathbf{F}_{\mathsf{elv}} = \begin{bmatrix} F_{\mathsf{elv,x}} \\ F_{\mathsf{elv,z}} \\ F_{\mathsf{elv,z}} \end{bmatrix} = \begin{bmatrix} 0 \\ 0 \\ 0 \end{bmatrix},$$

$$\mathbf{M}_{\mathsf{elv}} = \begin{bmatrix} L_{\mathsf{elv}} \\ M_{\mathsf{elv}} \\ N_{\mathsf{elv}} \end{bmatrix} = \begin{bmatrix} \bar{q} \, s_{\mathsf{elv}} b \, C_{L_{\mathsf{elv}}}(\delta_l, \delta_r) \\ \bar{q} \, s_{\mathsf{elv}} \bar{c} \, C_{M_{\mathsf{elv}}}(\delta_l, \delta_r) \\ 0 \end{bmatrix},$$

$$(8)$$

where  $\bar{q} = \frac{1}{2}\rho V_{\text{out}}^2$ .

 $C_{L_{\text{elv}}}(\delta_l, \delta_r)$  is a control derivative of  $L_{\text{elv}}$  expressed as a nonlinear function of  $\delta_l$  and  $\delta_r$ . Also,  $C_{M_{\text{elv}}}(\delta_l, \delta_r)$  is a nonlinear function that describes the control derivative of  $M_{\text{elv}}$ .

# 2.3.4 6DOF Equations of Motion

Combining (4), (7, and (8), the 6DOF equations of motion of the tailsitter can be formulated as shown,

$$\begin{split} \dot{u} &= rv - qw - g\sin\theta + \frac{F_{\text{wing},x}}{m} + \frac{F_{\text{prop},x}}{m} + \frac{F_{\text{elv},x}}{m}, \\ \dot{v} &= pw - ru + g\cos\theta\sin\phi + \frac{F_{\text{wing},y}}{m} + \frac{F_{\text{prop},y}}{m} + \frac{F_{\text{elv},y}}{m}, \\ \dot{w} &= qu - pv + g\cos\theta\cos\phi + \frac{F_{\text{wing},z}}{m} + \frac{F_{\text{prop},z}}{m} + \frac{F_{\text{elv},z}}{m}, \\ \dot{p} &= \frac{J_{yy} - J_{zz}}{J_{xx}}qr + \frac{L_{\text{wing}}}{J_{xx}} + \frac{L_{\text{prop}}}{J_{xx}} + \frac{L_{\text{elv}}}{J_{xx}}, \\ \dot{q} &= \frac{J_{zz} - J_{xx}}{J_{yy}}rp + \frac{M_{\text{wing}}}{J_{yy}} + \frac{M_{\text{prop}}}{J_{yy}} + \frac{M_{\text{elv}}}{J_{yy}}, \\ \dot{r} &= \frac{J_{xx} - J_{yy}}{J_{zz}}pq + \frac{N_{\text{wing}}}{J_{zz}} + \frac{N_{\text{prop}}}{J_{zz}} + \frac{N_{\text{elv}}}{J_{zz}}. \end{split}$$

With (9), we derived the full dynamic model with unknown function of aerodynamic coefficients.

# 3. Methodology

# 3.1 Sparse Identification of Nonlinear Dynamics

Consider a nonlinear dynamic system as:

$$\frac{d}{dt}\mathbf{x}(t) = \mathbf{f}(\mathbf{x}(t), \mathbf{u}(t)), \tag{10}$$

where  $\mathbf{x}(t) \in \mathbb{R}^n$  denotes system states,  $\mathbf{u}(t) \in \mathbb{R}^m$  denotes control inputs, and  $\mathbf{f}(\mathbf{x}(t))$  represents a nonlinear function of the states with dimension  $\mathbb{R}^n \times \mathbb{R}^l \to \mathbb{R}^n$ .

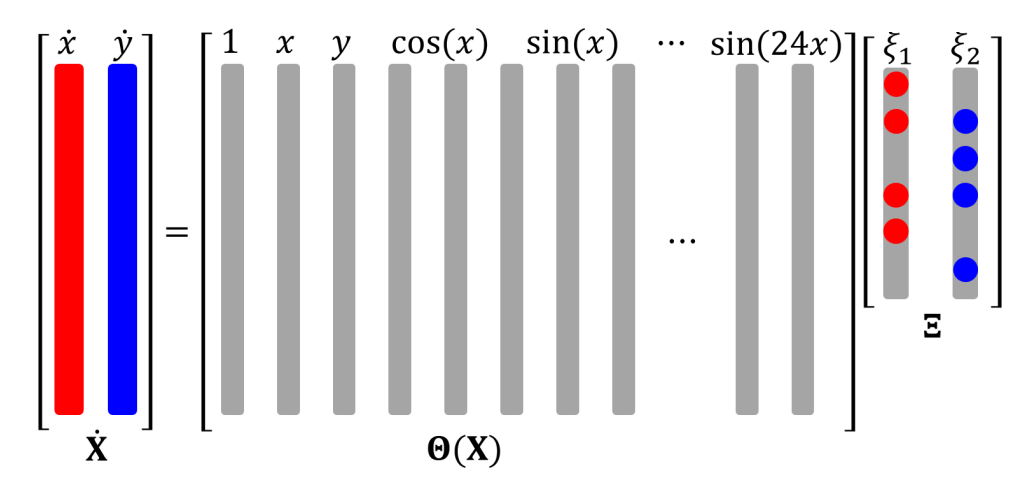


Figure 4 - Concept of SINDy.

To identify the unknown function  $\mathbf{f}$  from data, we collect a time history of the states  $\mathbf{x}(t)$  and the derivatives  $\dot{\mathbf{x}}(t)$  [13]. We assume all the required states and their derivatives are observable and collectable. The data can be arranged with time series into two matrices as follows:

$$\mathbf{X} = \begin{bmatrix} \mathbf{x}^{T}(t_{1}) \\ \mathbf{x}^{T}(t_{2}) \\ \vdots \\ \mathbf{x}^{T}(t_{m}) \end{bmatrix} = \begin{bmatrix} x_{1}(t_{1}) & x_{2}(t_{1}) & \dots & x_{n}(t_{1}) \\ x_{1}(t_{2}) & x_{2}(t_{2}) & \dots & x_{n}(t_{2}) \\ \vdots & \vdots & \ddots & \vdots \\ x_{1}(t_{m}) & x_{2}(t_{m}) & \dots & x_{n}(t_{m}) \end{bmatrix}, \, \dot{\mathbf{X}} = \begin{bmatrix} \dot{\mathbf{x}}^{T}(t_{1}) \\ \dot{\mathbf{x}}^{T}(t_{2}) \\ \vdots \\ \dot{\mathbf{x}}^{T}(t_{m}) \end{bmatrix} = \begin{bmatrix} \dot{x}_{1}(t_{1}) & \dot{x}_{2}(t_{1}) & \dots & \dot{x}_{n}(t_{1}) \\ \dot{x}_{1}(t_{2}) & \dot{x}_{2}(t_{2}) & \dots & \dot{x}_{n}(t_{2}) \\ \vdots & \vdots & \ddots & \vdots \\ \dot{x}_{1}(t_{m}) & \dot{x}_{2}(t_{m}) & \dots & \dot{x}_{n}(t_{m}) \end{bmatrix}. \quad (11)$$

And the library of candidate nonlinear functions are

where **X** is same data sets,  $\mathbf{X}^{p_2}, \mathbf{U}^{q_2}, \dots$  denote higher polynomials, and  $s_1, s_2, \dots$  represent frequencies of the sinusoidal functions.

Each column of  $\Theta(X,U)$  expresses a candidate function of the governing equation f and it can be arbitrarily selected to represent the nonlinearity effectively. The corresponding sparse vector of coefficients  $\xi_k$  comprises the below vector as shown in Fig. 4,

$$\Xi = \begin{bmatrix} \xi_1 & \xi_2 & \cdots & \xi_n \end{bmatrix}. \tag{13}$$

The system in (10) can be expressed in terms of data matrices as:

$$\dot{\mathbf{X}} = \Theta_{\text{total}}(\mathbf{X}, \mathbf{U}) \Xi_{\text{total}} + \eta \mathbf{Z} 
= \Theta_{\text{known}}(\mathbf{X}, \mathbf{U}) \Xi_{\text{known}} + \Theta(\mathbf{X}, \mathbf{U}) \Xi + \eta \mathbf{Z},$$
(14)

where  $\mathbf{Z}$  models the matrix of independently identically distributed Gussian noise with zero mean with magnitude  $\eta$ . Since the data  $\mathbf{X}$  and  $\dot{\mathbf{X}}$  are always contaminated with noise in realistic sense, it is reflected in (14). And in order to reduce the dimension and load of SINDy, the unknown model is divided from the known model which has determined parameters from existing knowledge.

Since most dynamical systems can be represented with few active terms in the governing equations, we will employ spare regression to identify the sparse matrix of coefficients  $\Xi$  signifying the fewest nonlinearities in  $\Theta(X)$  that results in a good model fit as:

$$\xi_{k} = \arg\min_{\xi_{k}} \frac{1}{2} \| \dot{X}_{k} - \xi_{k, \text{known}} \Theta_{\text{known}}^{T}(X_{k}, U_{k}) - \xi_{k} \Theta^{T}(X_{k}, U_{k}) \|_{2}^{2} + \lambda \| \xi_{k} \|_{1}$$
(15)

where  $\lambda$  is the regularizing parameter that make the our solution have a sparsity as a L1 penalty. Thus, it is converted into a problem of obtaining a spare solution of an overdetermined system with noise. The sparse vector of coefficients  $\xi_k$  can be found using the sequential threshold least square algorithm (STLS) [13]. With the optimization on (15), we can get the sparsed model representation of f by removing unwanted noise by adjusting the parameter  $\lambda$ .

# 3.2 Aerodynamic Model Identification

Combining the dynamics of tailsitter in (9) and aerodynamic models in (4), (7), and (8), the nonlinear dynamic model (10) of the tailsitter can be reconstructed as follows:

$$\begin{split} &\dot{u} = (rv - qw - g\sin\theta + \frac{T_l + T_r}{m})_{\text{known}} + (\frac{\bar{q}\,s_{\text{wing}}C_L(\alpha)\sin\alpha - \bar{q}\,s_{\text{wing}}C_D(\alpha)\cos\alpha}{m})_{\text{unknown}}, \\ &\dot{v} = (pw - ru + g\cos\theta\sin\phi)_{\text{known}}, \\ &\dot{w} = (qu - pv + g\cos\theta\cos\phi)_{\text{known}} + (\frac{-\bar{q}\,s_{\text{wing}}C_L(\alpha)\cos\alpha - \bar{q}\,s_{\text{wing}}C_D(\alpha)\sin\alpha}{m})_{\text{unknown}}, \\ &\dot{p} = (\frac{J_{yy} - J_{zz}}{J_{xx}}qr + \frac{c_Q(-T_l + T_r)}{J_{xx}})_{\text{known}} + (\frac{\bar{q}\,s_{\text{elv}}b\,C_{L_{\text{elv}}}(\delta_l,\delta_r)}{J_{xx}})_{\text{unknown}}, \\ &\dot{q} = (\frac{J_{zz} - J_{xx}}{J_{yy}}rp)_{\text{known}} + (\frac{\bar{q}\,s_{\text{wing}}\bar{c}\,C_M(\alpha) - (L\cos\alpha + D\sin\alpha)(x_{\text{ac}} - x_{\text{cg}}) + \bar{q}\,s_{\text{elv}}\bar{c}\,C_{M_{\text{elv}}}(\delta_{l,r})}{J_{yy}})_{\text{unknown}}, \\ &\dot{r} = (\frac{J_{xx} - J_{yy}}{J_{zz}}pq + \frac{l_{\text{prop}}(T_l - T_r)}{J_{zz}})_{\text{known}}, \end{split}$$

where  $(*)_{known}$  denotes the known model that is composed of observable states only and  $(*)_{unknown}$  represents the unknown model that contains the unknown function of aerodynamic coefficients. Using (16, the dynamic model can be expressed as

$$\dot{\mathbf{x}} = \mathbf{f}_0(\mathbf{x}, \mathbf{u}) + \mathbf{f}(\mathbf{x}, \mathbf{u}),\tag{17}$$

where  $\mathbf{f}_0$  is the known model and  $\mathbf{f}$  is the unknown model. Since the purpose of this paper is to identify the unknown aerodynamic coefficients, we utilize the existing knowledge of the model in (16). The unknown model is separated from the known model as a prior step and then SINDy is applied to the unknown model only. By moving the known model  $\mathbf{f}_0$  to the left side of (17), we can apply the SINDy for the unknown model  $\mathbf{f}$ . It reduces the size of the candidate function and helps to represent the aerodynamic model with fewer terms. Also, the constructed aerodynamic model can be clearly separated from the known model.

Reflecting the characteristics of the aerodynamic coefficients, the candidate function is chosen to be a set of constant, polynomials, and trigonometric functions since these functions have the universal function approximation property. To enhance the performance of sparse identification, the prior knowledge of the coefficients is be applied to the library selection. The lift, drag, and pitching moment functions are periodic functions that has a cycle of  $360^{\circ}$ . Also, they have symmetrical properties with respect to  $0^{\circ}$  AOA. It is also well known that the lift coefficient can be approximated as a linear function when it is not stalled. Thus, the lift coefficient function is divided in to post-stall region and unstalled region. With these prior knowledge, we suggest the basis of trigonometric function and polynomials to formulate the candidate function as:

where p is the order of polynomials of  $\mathbf{X}$  that range from 1 to 4, q is the order of polynomials of  $\mathbf{U}$  that range from 1 to 3, and  $\theta$  is the base frequency of the sinusoidal functions and the value of  $0.01^{\circ}$  is used for the given model.

### 4. Simulation Results

The state datasets for SINDy are generated through the 6DOF numerical simulation on Matlab. And the aerodynamic coefficient functions of the tailsitter is identified using the proposed method. To generate the dataset of the system, true dynamics are formulated using aerodynamic coefficients of NACA0012 airfoil obtained from wind tunnel analysis in [21]. The lift, drag, and pitching moment coefficient of NACA0012 from the wind tunnel data is used as a true value as shown in Fig. 5. For the control derivatives of the elevon model, a linear function is defined as a true model since we assumed the elevons actuate in unstalled condition.

Figure. 5 shows the result of SINDy analysis. It shows the identified aerodynamic coefficient function from measured data. Gaussian noise that has  $1\sigma$  at  $3^{\circ}/s$  is added on the angular velocity measurement  $\omega_B$  and Gaussian noise with  $1\sigma$  at  $0.1m/s(1\sigma)$  is applied on the linear velocity measurement  $\mathbf{v}_B$ .

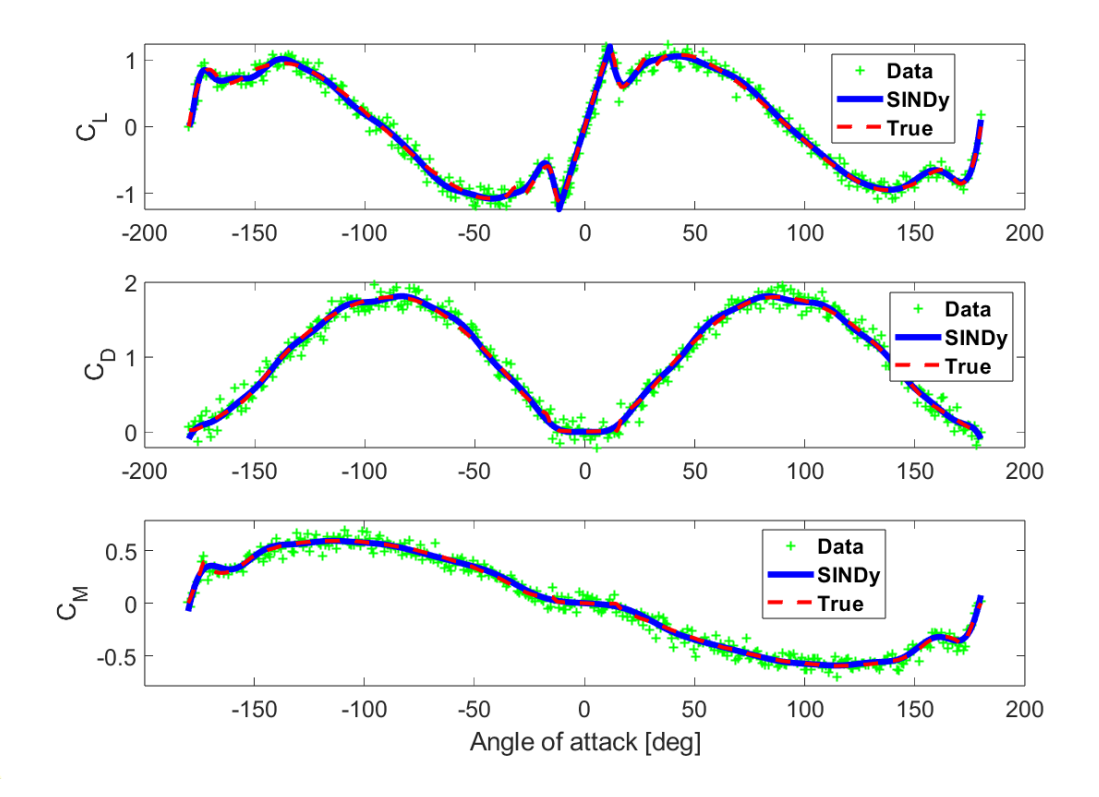


Figure 5 – Identified  $C_L, C_D, C_M$  from state measurement using SINDy.

Table. 2 shows the result of sparse regression. We can check that the initial sparse vector coefficients are reduced, leaving not more than 20 coefficients for the SINDy model. Therefore, the constructed model from SINDy represents the aerodynamic model with few active terms.

Table 2 – Reduced number of  $\xi$  of aerodynamic coefficients

f	C <sub>L (Linear)</sub>	C <sub>L</sub> (Nonlinear)	$C_D$	$C_M$	$C_{L_{elv}}$	$C_{M_{elv}}$
Number of unsparsed $\xi$	58	58	58	58	58	58
Number of sparsed $\xi$	1	20	16	15	1	1

Table. 3 shows the sparsed basis function and its coefficient. Since the  $C_D$  is symmetric with respect to  $\alpha = 0$ , the cosine functions with varying frequency remained with a constant term as a offset.

In order to check the validity of the identified SINDy model, a feedback linearization [22] based controller that uses a nonlinear dynamic model as a trim condition is implemented. The feedback linearization controller compensates the nonlinear aerodynamic model as a trim condition. And for

Table 3 – Sparsed basis function and its coefficient of  $C_D$ 

f				$C_D$				
Θ	1	$\cos(4\theta\alpha)$	$\cos(5\theta\alpha)$	$\cos(7\theta\alpha)$	$\cos(9\theta\alpha)$	$\cos(11\theta\alpha)$	$\cos(12\theta\alpha)$	$\cos(13\theta\alpha)$
Ξ	0.9664	-1.2978	0.5403	-0.3264	0.2875	-0.8241	1.3321	-0.9354
Θ	$\cos(15\theta\alpha)$	$\cos(17\theta\alpha)$	$\cos(18\theta\alpha)$	$\cos(20\theta\alpha)$	$\cos(21\theta\alpha)$	$\cos(22\theta\alpha)$	$\cos(23\theta\alpha)$	$\cos(24\theta\alpha)$
Ξ	0.4806	-0.7830	0.8897	-1.1554	1.7675	-1.4838	0.8031	-0.2428

the feedback control, three-loop structure is designed to deal with remaining model errors [23]. The forward transition flight where the longitudinal control is influenced by the aerodynamic model is simulated for 10 seconds. The initial pitch angle is  $80^{\circ}$  with zero speed. Then the pitch command of  $0^{\circ}$  and forward velocity command is set as 15m/s to keep steady level flight after the transition. In Fig. 6, the roll, pitch, yaw rate, and forward velocity in  $x_B$  is plotted. The control results of SINDy model are presented with the results of model error cases. Since there always exists modeling errors in actual flight, 10%, 20%, and 30% error is set to the aerodynamic coefficients and control derivatives of the elevon. We can check that the overshoot and damping are significantly decreased on the SINDy model when compared with the model error cases.

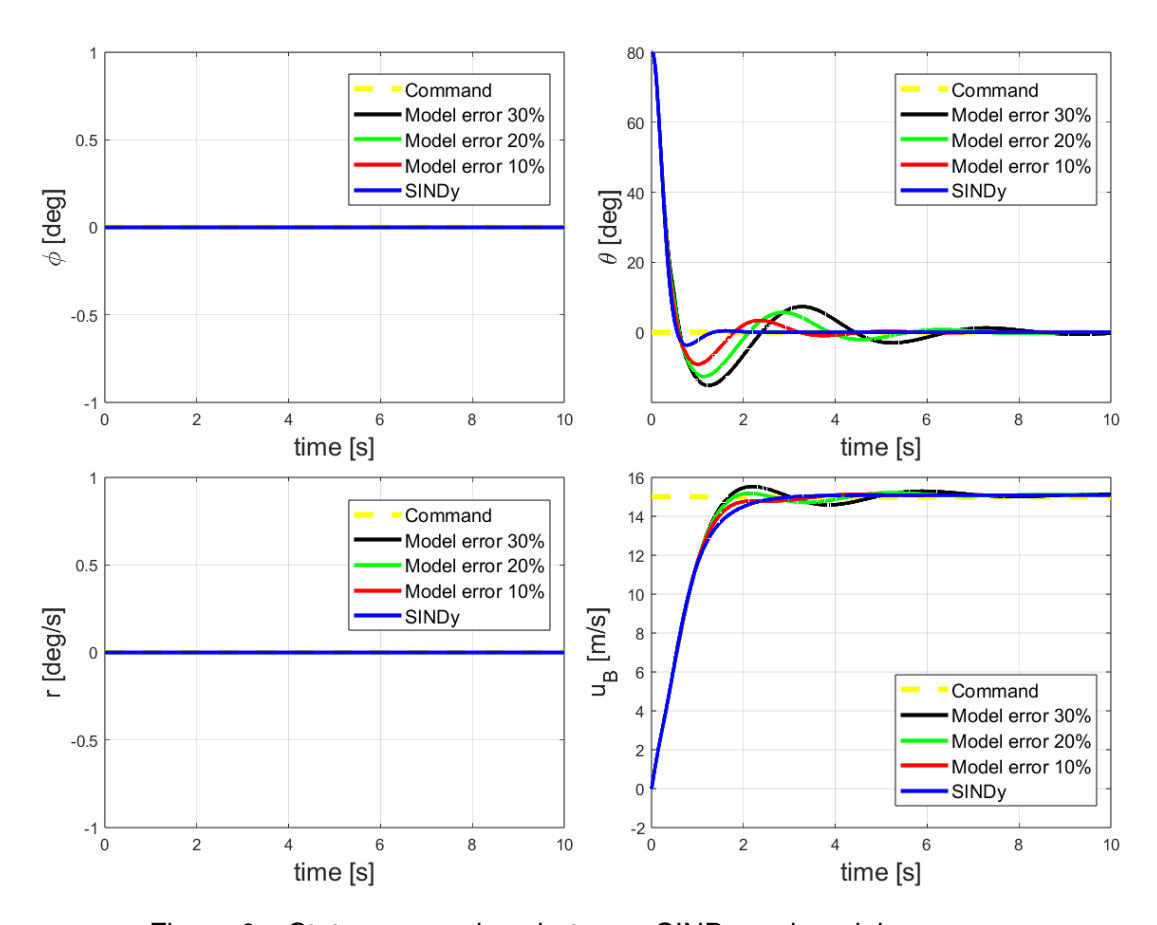


Figure 6 – States comparison between SINDy and model error cases.

The AOA, AOS, lift, and drag of the vehicle during forward transition is shown in Fig. 7. The SINDy model reduced the oscillation on lift and drag compared with the 10%, 20%, and 30% model error cases. It shows that the constructed the SINDy model represents the true aerodynamic model with less error.

# 5. Summary and Conclusion

In this paper, we designed an aerodynamic model identification of a tailsitter with flying wing configuration using Sparse Identification of Nonlinear Dynamics (SINDy). As a data-driven approach, SINDy

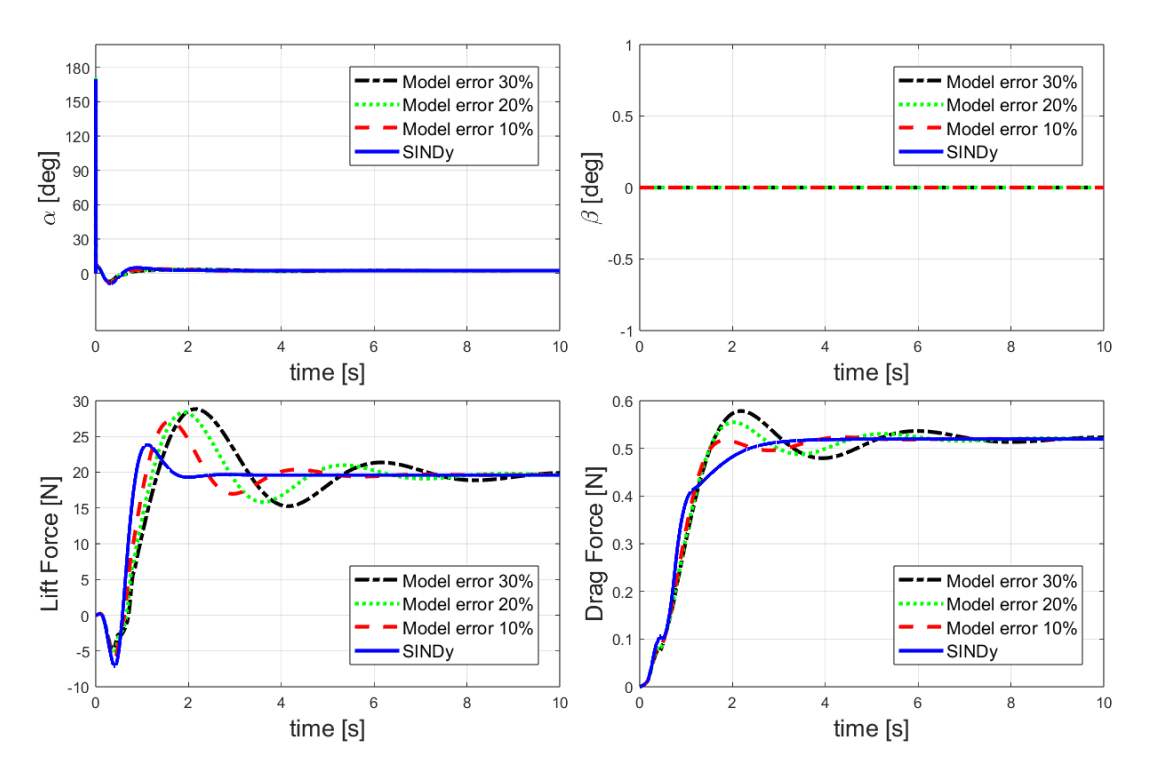


Figure 7 – Aerodynamics comparison between SINDy and model error cases.

was modeled to extract aerodynamic model based on the full dynamic model of the tailsitter. By utilizing the minimum knowledge of the model, SINDy identified the nonlinear functions of aerodynamic coefficients and control derivatives. The identified model was expressed with few active terms from the sparse solution. The SINDy model improved control performance when combined with feedback linearization controller. This approach can provide a new direction to utilize SINDy on aerodynamic model identification of VTOL aircrafts. Our future work will be to conduct a flight experiment to verify the proposed method.

### 6. Acknowledgements

This research was supported by Unmanned Vehicles Core Technology Research and Development Program through the National Research Foundation of Korea(NRF) and Unmanned Vehicle Advanced Research Center(UVARC) funded by the Ministry of Science and ICT, the Republic of Korea(2020M3C1C1A01083162)

### 7. Contact Author Email Address

If you have any questions, please send an email to: 'bbird222@kaist.ac.kr' (the first author) or 'hcbang@kaist.ac.kr' (corresponding author).

# 8. Copyright Statement

The authors confirm that they, and/or their company or organization, hold copyright on all of the original material included in this paper. The authors also confirm that they have obtained permission, from the copyright holder of any third party material included in this paper, to publish it as part of their paper. The authors confirm that they give permission, or have obtained permission from the copyright holder of this paper, for the publication and distribution of this paper as part of the ICAS proceedings or as individual off-prints from the proceedings.

### References

- [1] Guillaume JJ Ducard and Mike Allenspach. Review of designs and flight control techniques of hybrid and convertible vtol uavs. *Aerospace Science and Technology*, 118:107035, 2021.
- [2] Adnan S Saeed, Ahmad Bani Younes, Chenxiao Cai, and Guowei Cai. A survey of hybrid unmanned aerial vehicles. *Progress in Aerospace Sciences*, 98:91–105, 2018.

- [3] Sebastian Verling, Basil Weibel, Maximilian Boosfeld, Kostas Alexis, Michael Burri, and Roland Siegwart. Full attitude control of a vtol tailsitter uav. In *2016 IEEE international conference on robotics and automation (ICRA)*, pages 3006–3012. IEEE, 2016.
- [4] Robin Ritz and Raffaello D'Andrea. A global controller for flying wing tailsitter vehicles. In 2017 IEEE International Conference on Robotics and Automation (ICRA), pages 2731–2738, 2017.
- [5] Prasad Hemakumara and Salah Sukkarieh. Non-parametric uav system identification with dependent gaussian processes. In *2011 IEEE International Conference on Robotics and Automation*, pages 4435–4441, 2011.
- [6] Prasad Hemakumara and Salah Sukkarieh. Learning uav stability and control derivatives using gaussian processes. *IEEE Transactions on Robotics*, 29(4):813–824, 2013.
- [7] Kristofer Gryte, Richard Hann, Mushfiqul Alam, Jan Roháč, Tor Arne Johansen, and Thor I Fossen. Aerodynamic modeling of the skywalker x8 fixed-wing unmanned aerial vehicle. In *2018 International Conference on Unmanned Aircraft Systems (ICUAS)*, pages 826–835. IEEE, 2018.
- [8] Girish Chowdhary and Ravindra Jategaonkar. Aerodynamic parameter estimation from flight data applying extended and unscented kalman filter. *Aerospace science and technology*, 14(2):106–117, 2010.
- [9] Balakumaran Swaminathan, Joel George Manathara, and AK Vinayagam. Application of dynamic mode decomposition with control (dmdc) for aircraft parameter estimation. *IFAC-PapersOnLine*, 55(1):789–794, 2022.
- [10] Alejandro Flores and Gerardo Flores. Implementation of a neural network for nonlinearities estimation in a tail-sitter aircraft. *Journal of Intelligent & Robotic Systems*, 103(2):22, 2021.
- [11] Jingxuan Sun, Boyang Li, Chih-Yung Wen, and Chih-Keng Chen. Design and implementation of a real-time hardware-in-the-loop testing platform for a dual-rotor tail-sitter unmanned aerial vehicle. *Mechatronics*, 56:1–15, 2018.
- [12] Guibing Yang, Tao Wang, Ming Yang, Dengxiu Yu, and Zhen Wang. Adaptive tracking control for unknown dynamics systems with sindyc-based sparse identification. *Guidance, Navigation and Control*, 3(02):2350009, 2023.
- [13] Steven L Brunton, Joshua L Proctor, and J Nathan Kutz. Discovering governing equations from data by sparse identification of nonlinear dynamical systems. *Proceedings of the national academy of sciences*, 113(15):3932–3937, 2016.
- [14] Steven L Brunton, Joshua L Proctor, and J Nathan Kutz. Sparse identification of nonlinear dynamics with control (sindyc). *IFAC-PapersOnLine*, 49(18):710–715, 2016.
- [15] Urban Fasel, Eurika Kaiser, J Nathan Kutz, Bingni W Brunton, and Steven L Brunton. Sindy with control: a tutorial. In *2021 60th IEEE Conference on Decision and Control (CDC)*, pages 16–21. IEEE, 2021.
- [16] Mohamed Omar, Ruifeng Li, and Ahmed Asker. A framework for data driven dynamic modeling of serial manipulators. *IEEE Access*, 10:124874–124883, 2022.
- [17] Mohamed Omar, Ke Wang, Dai Kun, Ruifeng Li, and Ahmed Asker. Robust data-driven dynamic model discovery of industrial robots with spatial manipulation capability using simple trajectory. *Nonlinear Dynamics*, pages 1–23, 2024.
- [18] Jayden Dongwoo Lee, Sukjae Im, and Hyochoong Bang. Data-driven fault detection and isolation for quadrotor using sparse identification of nonlinear dynamics and thau observer. In *2024 International Conference on Unmanned Aircraft Systems (ICUAS)*, pages 382–389, 2024.
- [19] Dimitrios Papageorgiou, Guðrún Þóra Sigurðardóttir, Egidio Falotico, and Silvia Tolu. Sliding-mode control of a soft robot based on data-driven sparse identification. *Control Engineering Practice*, 144:105836, 2024.
- [20] Burak Yuksek, Aslihan Vuruskan, Ugur Ozdemir, MA Yukselen, and Gökhan Inalhan. Transition flight modeling of a fixed-wing vtol uav. *Journal of Intelligent & Robotic Systems*, 84:83–105, 2016.
- [21] Chris C Critzos, Harry H Heyson, and Robert W Boswinkle. *Aerodynamic characteristics of naca 0012 airfoil section at angles of attack from 0 to 180*. National Advisory Committee for Aeronautics, 1955.
- [22] Bernard Charlet, Jean Lévine, and Riccardo Marino. On dynamic feedback linearization. *Systems & Control Letters*, 13(2):143–151, 1989.
- [23] Young-Won Kim, Sang-Don Lee, Chang-Hun Lee, Hyo-Sang Shin, and Antonios Tsourdos. A nonlinear attitude controller for drones with cmg (control momentum gyro). In *2019 Workshop on Research, Education and Development of Unmanned Aerial Systems (RED UAS)*, pages 106–112. IEEE, 2019.